The heating and cooling of 2D electrons at low temperatures

A. K. Jain,[1] J. T. Nicholls,[1, a)] S. N. Holmes,[2] G. Jaliel,[3] C. Chen,[3] I. Farrer,[3, 4] and D. A. Ritchie[3]

[1)]*Physics Department, Royal Holloway, University of London, Egham TW20 0EX, United Kingdom*

[2)]*Department of Electronic and Electrical Engineering, University College London, Torrington Place, London WC1E 7JE, United Kingdom*

[3)]*Cavendish Laboratory, University of Cambridge, JJ Thomson Avenue, Cambridge, CB3 0HE, United Kingdom*

[4)]*Department of Electronic and Electrical Engineering, University of Sheffield, Mappin Street, Sheffield S1 3JD, United Kingdom*

(Dated: 21 August 2025)

We present measurements of the cooling length ℓ_E for hot electrons in a GaAs-based high mobility two-dimensional electron gas (2DEG). The thermal measurements are performed on a long 60 μm-wide channel, which is Joule-heated at one end, along which there are three similar hot-electron thermocouples, spaced 30 μm apart. The thermocouples measure an exponentially decaying temperature profile with a characteristic length ℓ_E, which decreases from 23 to 16 μm as the lattice temperature increases from 1.8 to 5 K. From a simple one-dimensional model of heat diffusion, we measure an inelastic scattering time which decreases from $\tau_i \approx 0.36$ to 0.18 ns. The measured τ_i has a magnitude and temperature dependence consistent with acoustic phonon scattering times. We discuss how the sample design can be varied for further thermal investigations. Knowledge of the temperature profile and its gradient will prove useful in measurements of the thermal conductivity and the Nernst effect.

The inelastic lifetime τ_i of an electron is an important quantity, as it determines how electrons in a device can dissipate their excess energy. Also, in quantum devices, the inelastic length scale is believed to provide the upper limit for the phase-breaking length.[1] In a GaAs-based two-dimensional electron gas (2DEG) of high electron mobility ($> 2 \times 10^6$ cm^2/Vs), the resistivity of a 2DEG increases linearly with temperature for $T \gtrsim 2$ K; a property that is determined by the thermal population of acoustic phonons available for scattering with the electrons. In thermal studies of 2DEGs, heated electrons lose their excess energy to the lattice by two routes: by inelastic electron-phonon scattering following a T^5 dependence in the Bloch-Gruneisen regime, or by a T^2 cooling by the Ohmic contacts. A crossover between the two was observed[2] using 1D electron thermometers at 0.3 K, and at lower temperatures using current noise thermometry.[3] In this work, we measure the thermal diffusion length using non-local heating; this directly gives the inelastic time τ_i, which we find to be determined by electron-phonon scattering.

In this work, the electrons are Joule heated by passing a current through the 2DEG. As the electron-electron relaxation length is much less than the sample dimensions, the electrons equilibrate to a local electron temperature T_e above the lattice temperature T_L, with a distribution that obeys Fermi-Dirac statistics. Previous electron thermometers in 2DEGs have been based on the temperature dependence of quantum corrections to the conductivity,[4] Johnson noise,[5] and the thermoelectric properties of 2D bar gates,[6] 1D[2] and 0D devices.[7] Chickering *et al.*[6] showed that an accurate hot-electron thermocouple (HET) can be created from a pair of bar gates which can measure the temperature T_e of the electrons in the channel when they are heated by as little as 10 mK above the lattice

[a)]Electronic mail: james.nicholls@rhul.ac.uk

temperature T_L. At low temperatures, the thermovoltage V_{th} developed across a single bar gate of the HET is given by

$$V_{th} = -S^d (T_e - T_L), \tag{1}$$

where S^d is the diffusion thermopower, which can be related to the electrical conductance G of a single bar gate using the Mott-Cutler relation[8]

$$S^d = -\frac{\pi^2 k_B^2}{3e} T \left(\frac{\partial \ln G}{\partial E} \right)_{E=E_F}, \tag{2}$$

where the energy derivative is determined at the Fermi energy E_F of the 2DEG. In the supplementary information (SI) we show a typical calibration using Eq. 2 of a single bar-gate; $\frac{\partial \ln G}{\partial E_F}$ is determined from $\frac{d \ln G}{d V_g} \frac{d V_g}{d E_F}$, where $G(V_g)$ is the measured conductance characteristic of the bar gate as a function of gate voltage V_g.

The diffusion thermopower S^d of a single bar gate can be written[6] as

$$S^d = -\frac{\pi^2 k_B}{3e} \frac{T}{T_F}(1+\alpha), \tag{3}$$

where T_F is the Fermi temperature (proportional to *n*). The quantity α is the elastic scattering parameter given by $\alpha = d(\ln \tau_e)/d(\ln n)$, describes the energy-dependent properties of the 2DEG, where τ_e is the elastic scattering time and *n* is the 2D electron density.

Devices were fabricated from two similar wafers (C2681 and T612) grown by molecular beam epitaxy. In both wafers the 2DEG is created 250 nm below the sample surface at the Al$_{0.33}$Ga$_{0.67}$As/GaAs interface; on top of the undoped GaAs there is 240 nm of Al$_{0.33}$Ga$_{0.67}$As, capped with a 10 nm GaAs top layer. There is Si-doping in the upper 200 nm of AlGaAs, giving a spacer layer distance of 40 nm between the dopants and the 2DEG. The main results presented in the figures is Device 1 from C2681 in which the mobility and carrier density

at 4.2 K are $\mu = 2.8 \times 10^6$ cm^2/Vs and $n = 1.5 \times 10^{11}$ cm^{-2}, with a resistance per square of $R_{sq} \approx 15$ Ω and a diffusivity $D = 1.44$ m^2/s. The elastic mean free path is 18 μm, and from the variation of n and μ with gate voltage we determine $\alpha \approx 1$. The properties of all samples investigated will be presented in Table I, later in the paper.

Figure 1 is a schematic of our T-shaped device which consists of two 60 μm wide channels, a heating (H) and a relaxation (R) channel. There are three similar HETs along the R-channel, positioned at x_1, x_2 and x_3, with thermocouple T3 positioned at x_3 shown in detail. From Eq. 3 the diffusion thermopower of T3 is $\Delta S^d \propto (1/n_1 - 1/n_2)$, where n_1 and n_2 are the 2D carrier densities under the two bar gates controlled by applied gate voltages V_{g1} and V_{g2}. Experiments show[6] that the measured thermopower ΔS of a HET follows the Mott-Cutler prediction (based on Eq. 2) for ΔS^d up to $T_L \approx 2$ K. At higher temperatures, $\Delta S = \Delta S^d + \Delta S^g$, is enhanced by a phonon drag contribution ΔS^g, such that $\Delta S^g \approx 0.35\ \Delta S^d$ at $T_L = 4$ K. See Ref. 6 and the SI for further details.

Using the Seebeck effect, we investigate the electron's excess temperature $\Delta T = T_e - T_L$ in both *local* and *non-local* measurements. When a heating current is passed along the R-channel the HETs act as local electron thermometers.[6] The cooling length ℓ_E is determined from *non-local* measurements of the excess electron temperature $\Delta T(x)$, using the set-up shown in Fig. 1. Electrons are heated in the H-channel and ΔT decays down the R-channel, as measured in previous studies.[4,9–12] Away from the heating current, the decay in $\Delta T(x)$ is characterized by a cooling length ℓ_E. In thermal diffusion the electrons exhibit an energy relaxation length, or cooling length, given by $\ell_E = \sqrt{D\tau_i}$ where the D is the diffusivity of the 2DEG. We will describe a method to measure ℓ_E, and hence τ_i.

In early work[4] on T-shaped devices the temperature decay in a 2D silicon inversion layer was used to determine its thermal conductivity. Previous studies[13] in a high-mobility 2DEG had only one working HET positioned 150 μm down the R-channel. A maximum cooling length of 250 μm was determined at 170 mK from the variations in the measured thermovoltage, as the carrier density under one of the 150 μm long bar gates was varied. In contrast, we will determine ℓ_E at higher temperatures using measurements of $\Delta T(x)$ from three HETs that are spaced 30 μm apart. Our bar gates are much longer ($L_g = 550$ μm) than the measured ℓ_E, thus simplifying the analysis.

In the non-local heating set-up an AC current $I_H \sin(\omega t)$ of frequency $f = \omega/(2\pi) = 64$ Hz is passed through the H-channel. Due to Joule heating, electrons in the middle of the H-channel at $x = 0$ will have an oscillating electron temperature

$$T_e = T_L + \Delta T_0 \left[1 - \cos(2\omega t)\right]. \qquad (4)$$

For small AC heating currents, when $T_L \gg \Delta T_0$, the electrons will have an excess temperature $\Delta T = T_e - T_L$, that oscillates with frequency $2f$ with a phase shift of $\pi/2$. It is assumed that the electrons in the large area (250μm×150μm) AuNiGe Ohmic contacts, with a contact resistance of ~ 50 Ω, are anchored to the lattice temperature T_L. Due to heating of the

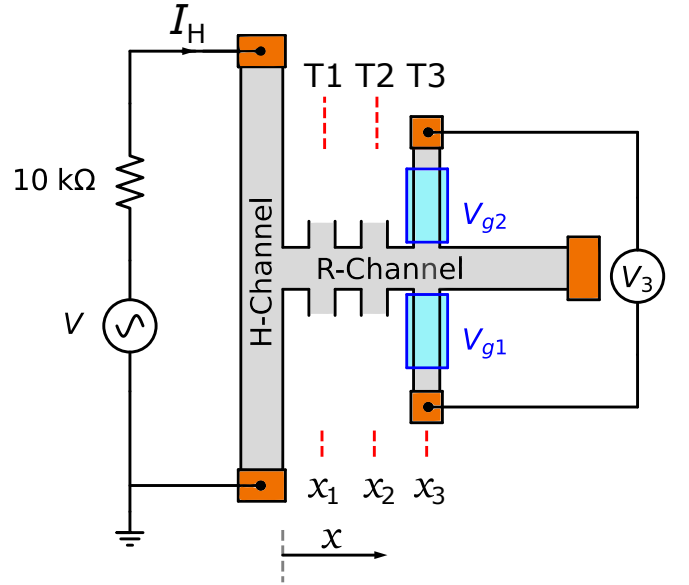FIG. 1. Schematic of the T-shaped device, which consists of 60 μm wide heating (H) and relaxation (R) channels, with lengths 720 μm and 600 μm, respectively. All Ohmic contacts in the device (shown in orange) are thermally grounded to the lattice temperature T_L. In *non-local* measurements, an AC heating current of amplitude I_H and frequency f is driven between the Ohmic contacts on the H-channel; all other contacts in the device are electrically floating. Due to heating by I_H, the electrons at the midpoint of the H-channel at $x = 0$ are heated above T_L by an excess temperature ΔT_0. The excess temperature, $\Delta T(x) = T_e(x) - T_L$, along the R-channel decreases with increasing x, and is measured using three similar hot-electron thermocouples (HETs) centered at $x_1 = 22.5$ μm, $x_2 = 52.5$ μm and $x_3 = 82.5$ μm. Thermocouple T3 is shown in detail; it consists of two 15 μm wide voltage probes, in which the electron carrier densities n_1 and n_2 can be varied using voltages V_{g1} and V_{g2} applied to surface gates of length $L_g = 550$ μm.

electrons in the R-channel between the voltage probes of T3, a thermovoltage V_3 at frequency $2f$ is measured between the two Ohmic contacts.

Figure 2(a) shows the thermovoltage V_3 at $T_L = 4.0$ K, as a function of a *local* heating current I_R passed through the R-channel. V_3 follows a quadratic dependence on heating current, $V_3 = a_3 I_R^2$, where $a_3 = 3.69$ nV/(μA)^2. Similar thermovoltage characteristics were obtained for the T1 and T2 thermocouples, which were operated at the same bar gate voltages as T3. The fitted values for a_1, a_2 and a_3 are within 6% of each other, and have been used to fine-tune the calibrations of the HETs when they are used for relative thermometry measurements in the non-local geometry.

In *non-local* measurements, the electrons in the H-channel are heated by a current I_H, which sets up a temperature gradient along the R-channel, driving diffusive heat flow in the x-direction. In a simple one-dimensional description,[14] the excess temperature $\Delta T(x)$ is governed by the differential equation:

$$\kappa \frac{d^2(\Delta T(x))}{dx^2} - \frac{C_e \Delta T(x)}{\tau_i} = 0, \qquad (5)$$

where κ is the thermal conductivity, and C_e is the electron heat capacity. If the R-channel is much longer than ℓ_E, the solution to Eq. 5 is an exponential decay

$$\Delta T(x) = \Delta T_0 \exp(-x/\ell_E), \qquad (6)$$

with prefactor ΔT_0, the excess temperature at $x = 0$, and characterized by the cooling length $\ell_E = \sqrt{\kappa \tau_i / C_e}$. This length can be written[14,15] as

$$\ell_E = \sqrt{D \tau_i}, \qquad (7)$$

where $D = v_F^2 \tau_e / 2$ is the 2D diffusivity, v_F is the Fermi velocity, and τ_e is the elastic scattering time.

In non-local measurements the excess temperature $\Delta T(x)$ generates thermovoltages in the HETs along the R-channel. Figure 2(b) shows non-local measurements of V_1, V_2 and V_3 at $T_L = 4.0$ K; similar to local measurements there are good fits to the quadratic form $V_i = b_i I_H^2$, with the values of b_i given in the figure. The most important feature is the diminishing effect of I_H on V_i as x increases. If a similar calibration for all the HETs is assumed from the local measurements in Fig. 2(a), then the exponential decay in $\Delta T(x)$ described by Eq. 6 will also be measured in the thermovoltages such that

$$V_i = \Delta S \Delta T(x_i) = \Delta S \Delta T_0 \, e^{-x_i/\ell_E}, \qquad (8)$$

where ΔS is the magnitude of the thermopower of the three similar HETs. From measurements of the ratio V_j/V_i, the cooling length ℓ_E can be obtained from $\ell_E = (x_i - x_j)/\ln(V_j/V_i)$, which is derived from Eq. 8. Three possible measurements of ℓ_E are:

$$\ell_E = \frac{30 \, \mu\text{m}}{\ln(V_1/V_2)}, \quad \ell_E = \frac{30 \, \mu\text{m}}{\ln(V_2/V_3)}, \quad \text{and} \quad \ell_E = \frac{60 \, \mu\text{m}}{\ln(V_1/V_3)}, \qquad (9)$$

which are plotted in Fig. 2(c) as a function of I_H. For $I_H < 15 \, \mu\text{A}$ the V_j/V_i ratios show fluctuations; at higher I_H these diminish and the three plots settle to give $\ell_E = 15.8 \pm 0.3 \, \mu\text{m}$.

When the local and non-local measurements were performed at $T_L = 1.8$ K, the electron-phonon cooling is diminished and the cooling length ℓ_E increases. At 1.8 K the HETs show similar characteristics in local heating and in Figs. 3(a) and (b) we present non-local measurements of V_1, V_2 and V_3, and the cooling length ℓ_E determined from their ratios. The behavior of $\Delta T(x)$ is not perfectly exponential, as shown by the $\sim 1 \, \mu\text{m}$ difference in ℓ_E obtained from the V_j/V_i ratios; the black horizontal line shows the cooling length $\ell_E = 22.7 \pm 1.0 \, \mu\text{m}$, which is determined from the average of the three ratios. As the temperature is further reduced (not shown) deviations from exponential behavior become more apparent, consistent with relatively stronger cooling by the Ohmic contacts as the electron-phonon interaction weakens.

Due to the current I_H flowing in the H-channel, one end of the R-channel is heated, and Figs. 2 and 3 show an exponential decay of the excess temperature $\Delta T(x) \propto e^{-x/\ell_E}$, characterized by the length scale ℓ_E. The functional dependence of the three thermovoltages on I_H are similar, being all determined by ΔT_0,
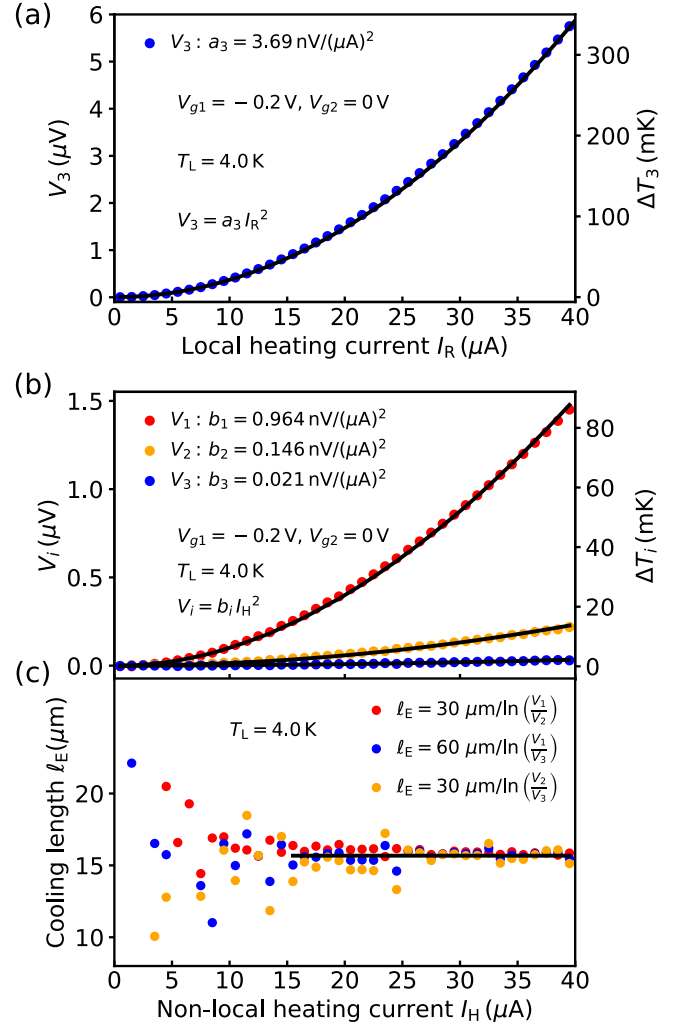

FIG. 2. Measurements of thermovoltages at $T_L = 4.0$ K, when the gate voltages on all three HETs were set to $V_{g1} = -0.2$ V and $V_{g2} = 0$ V. The Joule heating was either in the *local* or *non-local* geometries shown in the insets; in both cases good fits were obtained to parabolic forms. (a) In local measurements only the thermovoltage V_3 is plotted, with a parabolic fit $V_3 = a_3 I_R^2$ up to 40 μA, where $a_3 = 3.69$ nV/$(\mu\text{A})^2$. T1 and T2 have similar characteristics, with $a_1 = 3.62$ nV/$(\mu\text{A})^2$ and $a_2 = 3.47$ nV/$(\mu\text{A})^2$. (b) In non-local measurements, the thermovoltages of the HETs show a decreasing response to I_H as x increases. (c) The cooling length ℓ_E is determined from the data points in (b) using the three expressions in Eq. 9. For $I_H > 20 \, \mu$A, the cooling length is $\ell_E = 15.8 \pm 0.3 \, \mu$m at 4.0 K. The estimated temperatures ΔT_i given on the right hand side of (a) and (b) are calculated using an electron-phonon cooling time of $\tau_{ep} = 1$ ns$/T$ (in K); see SI for details.

which is the excess temperature at the centre of the H-channel at the $x = 0$. At $T_L = 4.0$ K, when electron-phonon cooling is strong, the electron temperature at the centre of a simple bar, well away from the Ohmic contacts, is constant, and ΔT_0 is proportional to the Joule heating $I_H^2 R_{sq}$. At $T_L = 1.8$ K the thermovoltages V_i follow I_H^2 behavior for $I_H < 12 \, \mu$A, but for
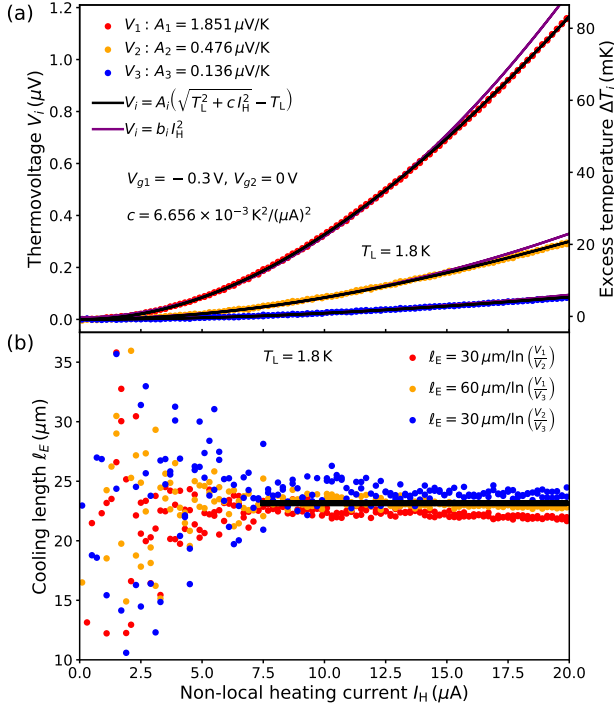
FIG. 3. (a) Non-local measurements of the thermovoltages V_1, V_2, and V_3 at $T_L = 1.8$ K as a function of the heating current I_H. Fits to Eq. 10 give the values of A_i and c shown in the figure. The excess temperatures ΔT_1, ΔT_2 and ΔT_3 on the right hand vertical axis, are calculated from calibrations based on the Mott-Cutler relation. (b) The ratios of V_i/V_j as a function of I_H are used to determine a cooling length $\ell_E = 22.7 \pm 1.0$ μm at 1.8 K.

$I_H < 20$ μA there is a better least-squares fit to

$$V_i = A_i \Delta T_0 = A_i \left(\sqrt{T_L^2 + c I_H^2} - T_L \right), \qquad (10)$$

a functional form used in hot-electron studies of diffusive metal wires.[16,17] Figure 3(a) shows the best fits, where A_i and c are fitting parameters. Using $c = 0.0665$ (K/μA)^2 the fits of V_1, V_2 and V_3 to Eq. 10 are surprisingly good at $T_L = 1.8$ K.

Figure 4 shows the length ℓ_E measured for different lattice temperatures T_L, when the gate voltages on all three HETs were set at $V_{g1} = -0.3$ V and $V_{g2} = 0$ V. At temperatures above 2 K, the electron-phonon mechanism is the expected source of inelastic scattering. It is well known that in GaAs-based 2DEGs the scattering from acoustic phonons gives rise to the linear temperature dependence of the resistivity $\rho(T)$ in high mobility 2DEGs for $T \gtrsim 2$ K. To fit ℓ_E for $T_L > 1.8$ K, we have assumed that the inelastic time is equal to the electron-phonon scattering time:

$$\tau_i = \tau_{ep} = \frac{B \times 1 \text{ ns}}{T (\text{in K})}, \qquad (11)$$

where the 1 ns/T(in K) term comes from Ref. 18, assuming a 2DEG width of $d = 10$ nm. A best fit $B = 0.69 \pm 0.02$ is obtained for temperatures $T_L \geq 1.8$ K, giving electron-phonon
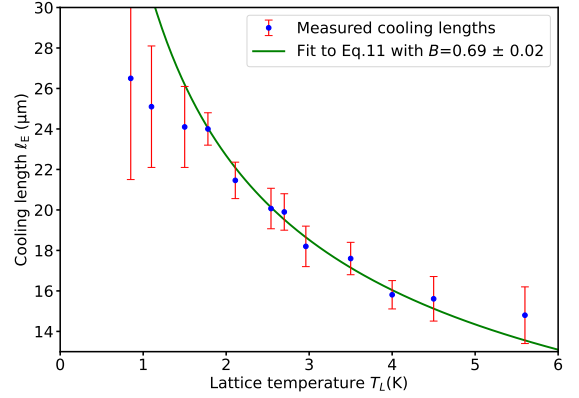

FIG. 4. The cooling length ℓ_E measured at different lattice temperatures T_L. Assuming that τ_i is equal to τ_{ep} with the form given in Eq. 11, the best fit with $B = 0.69 \pm 0.02$ is obtained for $T_L \geq 1.8$ K.

scattering times similar to those obtained from $\rho(T)$ measurements.

Four different devices were investigated, with electrical and thermal results at $T_L = 4.2$ K summarized in Table I. Devices 1 and 2 were fabricated from wafer C2681 using the same mask set, where the heating channel and the relaxation channel are both 60 μm wide. The measured τ_i at 4.2 K are very close for the two devices, and the value $B = 0.687$ is consistent with measurements in Fig. 4. Devices 3 and 4 were fabricated from wafer T612, which has similar growth parameters to C2681, using a mask set with a 60 μm-wide heating channel, but with different widths for the voltage probes (w) and the relaxation channel (W). Despite the variation in n and μ, the measured inelastic times are in close agreement; further evidence that τ_i depends only the lattice temperature (see Eq. 11). We argue in the next paragraph that the slightly higher values of τ_i in Devices 3 and 4 are caused by the narrower widths of the voltage probes.

To use HETs in different studies, for example to map out the temperature profile $T_e(x)$ along the relaxation channel at lower temperatures, a number of design issues should be considered:

(i) **the width W of the relaxation channel** In non-local measurements, a small fraction of I_H extends into the R-channel. This is characterized by the non-local resistance $R_{nl} = V_t/I_H$, where V_t is the voltage measured across the R-channel at position x, which theory predicts[19] will decay exponentially down the R-channel as:

$$R_{nl} = F R_{sq} \exp(-x\pi/W), \qquad (12)$$

where F is a geometric factor of order unity. For $W = 60$ μm the voltage relaxation length is $W/\pi \approx 19$ μm; this has been confirmed experimentally by V_t measurements at x_1, x_2 and x_3 where $F \approx 0.5$, in agreement with a simple finite element model of the electrostatics. Therefore, the parasitic electron heating in the R-channel will extend over a length $W/(2\pi) \approx 10$ μm, which is smaller than any measured cooling length. The results from Device 3 show that ℓ_E is not

Device	n ($\times 10^{11}\,\mathrm{cm}^{-2}$)	μ ($\times 10^{6}\,\mathrm{cm}^2/\mathrm{Vs}$)	W (μm)	w (μm)	D (m^2/s)	ℓ_{E} (μm)	τ_i (ns)
1	1.50	2.82	60	15	1.51	15.7±0.3	0.163±0.006
2	1.50	2.91	60	15	1.58	16.1±0.2	0.164±0.004
3	2.51	2.18	30	10	1.95	18.5±0.2	0.176±0.004
4	2.66	2.27	60	5	2.16	20.0±0.5	0.185±0.009

TABLE I. Properties of the four devices measured at $T_L = 4.2$ K. w is the width of the voltage probes and W is the width of the relaxation channel. Measurements from Device 1 are shown in Figs. 2-4.

changed when the width W is reduced to 30 μm, so we believe that parasitic heating is not affecting our results.

(ii) **the width w of the HET probes** The HET voltage probes are paths for heat to leak out of the relaxation channel. Finite element model simulations show that the measured ℓ_{E} and τ_i will be lowered as the width w increases, numbers typically being 5% for ℓ_{E} and 10% for τ_i. This explains the trend that the measured τ_i is higher for Devices 3 and 4 compared to Devices 1 and 2. To make more accurate inelastic scattering time measurements, the smallest possible w should be used, and the HETs should be run at more negative gate voltages.

(iii) **the spacing of the HET probes** If the temperature is lowered to dilution fridge temperatures the exponential temperature profile, $\Delta T(x) \sim \exp(-x/\ell_{\mathrm{E}})$, will be replaced by one that is determined by cooling by the Ohmic contacts on the HET voltage probes, as well as the Ohmic contact at the far end of the R-channel. To accurately measure the temperature profile in this limit requires HETs spaced evenly along the R-channel.

In conclusion, we show how bar gate thermometers can be used to measure the cooling length ℓ_{E}, wth a method that is applicable to other 2D materials which are gatable. Spatially separating the heating and cooling in non-local measurements is key to measuring the inelastic scattering time τ_i. For $T_L =$ 2-5 K the measured τ_i has no dependence on carrier density n, but follows the temperature dependence for inelastic scattering by acoustic phonons. As the lattice temperature T_L is reduced below 2 K cooling by the lattice diminishes, and cooling by the Ohmic contacts become more dominant. This crossover in cooling mechanism leads to a non-exponential temperature profile in the relaxation channel. Consistent with this crossover, for $T_L < 2$ K there is no phonon drag contribution (ΔS^g) to the measured thermopower of the bar gates, and the 2DEG resistivity $\rho(T)$ saturates to a constant value that is determined by the electron-impurity scattering.

Measurements of $\Delta T(x)$ also provide information about the temperature gradient, $\nabla T(x)$, a quantity that determines the magnitude of the magneto-thermopower in a transverse magnetic field, which will be presented elsewhere.[20]

Supplementary Material See supplementary information (SI) file for further information.

Data availability: The data that support the findings of this study are available from the corresponding author upon reasonable request.

[1] J. J. Lin and J. P. Bird, J. Phys.: Cond. Matt. **14**, R501 (2002).
[2] N. J. Appleyard, J. T. Nicholls, M. Y. Simmons, W. R. Tribe, and M. Pepper, Phys. Rev. Lett. **81**, 3491 (1998).
[3] L. V. Levitin et al., Nature Commun. **13**, 667 (2022).
[4] R. T. Syme, M. J. Kelly, and M. Pepper, J. Phys.: Cond. Matt. **1**, 3375 (1989).
[5] C. Kurdak, D. C. Tsui, S. Parihar, S. A. Lyon, and M. Shayegan, Appl. Phys. Lett. **67**, 386 (1995).
[6] W. E. Chickering, J. P. Eisenstein, and J. L. Reno, Phys. Rev. Lett. **103**, 046807 (2009).
[7] A. Mavalankar et al., Appl. Phys. Lett. **103**, 133116 (2013).
[8] M. Cutler and N. F. Mott, Phys. Rev. **181**, 1336 (1969).
[9] F. L. Bakker, J. Flipse, and B. J. van Wees, J. Appl. Phys. **111**, 084306 (2012).
[10] J. F. Sierra, I. Neumann, M. V. Costache, and S. O. Valenzuela, Nano Lett. **15**, 4000 (2015).
[11] V. Narayan, M. Pepper, and D. A. Ritchie, C. R. Phys. **17**, 1123 (2016).
[12] J. Waissman et al., Nat. Nanotechnol. **17**, 166 (2021).
[13] J. Billiald et al., Appl. Phys. Lett. **107**, 022104 (2015).
[14] S. Rojek and J. König, Phys. Rev. B **90**, 115403 (2014).
[15] M. Massicotte, G. Soavi, A. Principi, and K.-J. Tielrooij, Nanoscale **13**, 8376 (2021).
[16] M. Henny et al., Appl. Phys. Lett. **71**, 773 (1997).
[17] B. Huard, H. Pothier, D. Esteve, and K. E. Nagaev, Phys. Rev. B **76**, 165426 (2007).
[18] V. K. Arora and A. Naeem, Phys. Rev. B **31**, 3887 (1985).
[19] D. A. Abanin, A. V. Shytov, L. S. Levitov, and B. I. Halperin, Phys. Rev. B **79**, 035304 (2009).
[20] A. K. Jain et al., in preparation, 2025.